Insight into the Alkaline Stability of Arylene-Linked Bis-Benzimidazoles and Polybenzimidazoles

Serhiichuk, Dmytro; Patniboon, Tipaporn; Xia, Yifan; Kraglund, Mikkel Rykær; Jensen, Jens Oluf; Hansen, Heine Anton; Aili, David

Published in:
ACS Applied Polymer Materials

Link to article, DOI:
10.1021/acsapm.2c01769

Publication date:
2023

Document Version
Peer reviewed version

Insight into the alkaline stability of arylene-linked bis-benzimidazoles and polybenzimidazoles

Dmytro Serhiichuk,[‡] Tipaporn Patniboon,[‡] Yifan Xia, Mikkel Rykær Kraglund, Jens Oluf Jensen, Heine Anton Hansen, David Aili[*]

Department of Energy Conversion and Storage, Technical University of Denmark, Elektrovej, Building 375, 2800 Kgs. Lyngby, Denmark, [*]Corresponding author (E-mail: larda@dtu.dk)

KEYWORDS

Polybenzimidazole, stability, degradation, model system, alkaline electrolyte

ABSTRACT

Polybenzimidazole doped with aqueous KOH has emerged as an attractive electrolyte system for high-rate alkaline water electrolysis, since it combines high ion conductivity with low H_2 permeability. The lifetime is, however, limited to a few weeks under operating conditions due to degradation modes leading to chain scission. In this work, the underlying degradation mechanisms are explored by monitoring the chemical changes of a series of small molecule arylene linked bis-benzimidazoles treated under extreme caustic conditions for nearly 6 months at 80 °C. Degradation products and degradation pathways are identified experimentally and supported by density functional theory calculations. Based on the experimental and theoretical data, it is suggested that the degradation mainly proceeds via the remaining fraction of neutral benzimidazole and that stability can be improved by increasing the degree of deprotonation along the molecule.

1 INTRODUCTION

The polybenzimidazoles are a large family of engineering polymers with a structural scope that has grown tremendously during the past decades.[1] The design and synthesis of new polybenzimidazole derivatives has primarily been driven toward fuel cell applications in combination with phosphoric acid doping.[2] The recent development of flow battery,[3] water electrolysis[4,5] and gas separation[6] technologies continue to stimulate the development of new polybenzimidazole chemistries, functionalization strategies and composite materials approaches.

The chemical environment that the polybenzimidazoles experience in these applications is typically a high-ionic strength aqueous solution with extreme pH. Due to the amphoteric nature of the benzimidazole groups, the polymer responds to the chemical environment changes by protonation/deprotonation, as exemplified in Scheme 1. In an acidic environment, the protic

benzimidazolium (i) predominates[7] while the deprotonated benzimidazolide form (ii) has been found to predominate under extreme caustic conditions.[8] The dialkylbenzimidazolium salts, which are synthesized by full *N*-alkylation or *N*-arylation of the benzimidazoles,[9] can be obtained in the dihydrogen phosphate (iii) or hydroxide (iv) forms through anion exchange.

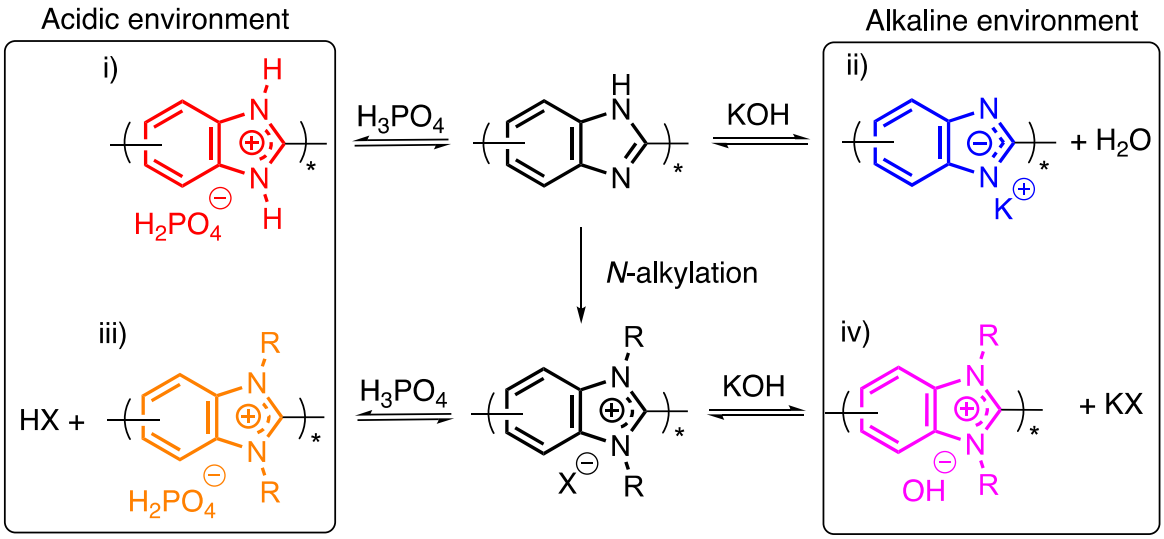

Scheme 1. Benzimidazole units of a generic polybenzimidazole in the protic benzimidazolium form (i), potassium benzimidazolide form (ii), dialkylbenzimidazolium dihydrogen phosphate form (iii) and dialkylbenzimidazolium hydroxide form (iv).

When it comes to device integration, long-term chemical stability is one of the most critical parameters that needs to be considered. Recent model system studies show that protic benzimidazolium (i) as well as *N*,*N*′-dimethylbenzimidazolium (iii) are fully stable in 85% H_3PO_4 at 160 ºC for 20 days.[10] On the other hand, *N*,*N*′-dimethylbenzimidazolium salts in the hydroxide form (iv) experience rapid degradation due to hydrolysis at the benzimidazolium C2 position and severe stability limitations at the polymer level.[11] Chemical stability is a general challenge for

organic cations in alkaline environment due to their electrophilic nature, and degradation mechanisms and stability windows are relatively well understood.[12,13] With this knowledge, successful degradation mitigation strategies have been developed and materialized as alkali-resistant anion exchange membrane chemistries derived from e.g. poly(arylene imidazolium)s,[14,15] poly(arylene benzimidazolium)s,[16,17] poly(arylene piperidinium)s,[18,19] poly(arylene alkylene)s,[20] polyphenylenes[21] or radiation grafted polyolefins.[22] As mentioned above, the *N*,*N*′-dialkylbenzimidazolium cations are highly electrophilic around the benzimidazolium C2 position, and steric hinderance has proven very effective at preventing nucleophilic attack by hydroxide ions as demonstrated at the polymer level[16,17] and supported by small-molecule model system studies and simulations.[23] The degradation can be further mitigated by crosslinking[24,25] and computational studies show that inductive effects from electron rich adjacent groups effectively contribute to suppressing the degradation of sterically protected *N*,*N*′-dialkylbenzimidazolium.[26]

The benzimidazolide salts (iii), on the other hand, carry a negative charge which intuitively should result in reduced electrophilicity around the C2 position. This seems supported by recent computations,[27] and the chemical stability has been assessed at the polymer level in 5-50 wt.% KOH at 88 ºC.[28] From the experimental work, the molecular weight was found to decrease over time, and the rate of molecular weight decrease was found to increase with increasing KOH concentration. Similar studies have been carried out with derivatives that are linked with steric trimethylphenyl units[29] or bulky naphthalene groups,[30] and the results point in the same direction. However, while non-protected poly(dialkylbenzimidazolium)s rapidly degrade completely by ring opening and chain scission at the time scale of hours[9,11] the poly(benzimidazolide)s show a stability window of months.[28,31]

It has been hypothesized that the degradation of benzimidazolides in alkaline media occurs via a similar pathway as the degradation of the dialkylbenzimidazoliums, starting by nucleophilic attack at the benzimidazolide C2 position followed by ring opening and amide hydrolysis.[29,31] However, recent computational studies point out that the degradation pathway likely proceed from the small fraction of neutral benzimidazole units, which are considerably more electropositive than the deprotonated benzimidazolide form.[27] This work aims at shedding light on the stability of benzimidazole derivatives in alkaline media, by monitoring the chemical changes of a series of model compounds in aqueous alkaline environment for more than 3000 h and correlating the experimental results with data from simulations.

2 EXPERIMENTAL

2.1 Materials

Benzene-1,3-dicarboxylic acid, benzene-1,4-dicarboxylic acid, 5-hydroxybenzene-1,3-dicarboxylic acid, 4,4′-dicarboxydiphenyl ether, 4,4′-(hexafluoroisopropylidene)bis(benzoic acid), 1,2-diaminobenzene, polyphosphoric acid (PPA), ortho-phosphoric acid (PA, 85 wt.%), methanol-d_6 (MeOD), potassium deuteroxide (KOD, 40 wt.% in D_2O), deuterium oxide (D_2O) and sodium hydroxide were all purchased from Sigma-Aldrich and used as received.

2.2 Synthesis of model compounds

1,3-bis(1*H*-benzo[*d*]imidazol-2-yl)benzene (1) A three-neck round-bottomed flask equipped with a magnetic stirrer, a water cooled condenser and an argon inlet and outlet was charged with 1,2-diaminobenzene (1.30 g, 12.00 mmol), benzene-1,3-dicarboxylic acid (1.00 g, 6.00 mmol), 30 mL PPA and 15 mL of PA. The temperature was slowly raised to 200 ºC and the reaction mixture

was heated for 6 h. The resulting solution was allowed to cool slowly to room temperature and subsequently poured into cold water, followed by addition of NaOH flakes to pH = 8. The precipitate was filtered off, washed with water and dried. The crude product was recrystallized from methanol and dried under vacuum at 60 ºC to give 1 as a light-brown solid (1.51 g, 90% yield). ^{1}H NMR (80 MHz, DMSO-d_6) δ 9.05 (1 H, d, J = 1.9 Hz), 8.27 (2 H, dd, J = 7.6, 1.7 Hz), 7.91-7.42 (5 H, m), 7.26 (4 H, dt, J = 6.0, 3.5 Hz).

1,4-bis(1*H*-benzo[*d*]imidazol-2-yl)benzene (2) Synthesized as described for **1**, from 1,2-diaminobenzene (1.30 g, 12.00 mmol) and benzene-1,4-dicarboxylic acid (1.00 g, 6.00 mmol). **2** was as isolated as light-brown solid after recrystallization from methanol (1.42 g , 85% yield). ^{1}H NMR (80 MHz, DMSO-d_6) δ 13.16 (2 H, s), 8.48 (4 H, s), 7.75 (4 H, m), 7.35 (4 H, m).

3,5-bis(1*H*-benzo[*d*]imidazol-2-yl)phenol (3) Synthesized as described for **1**, from 1,2-diaminobenzene (1.20 g, 11.00 mmol) and 5-hydroxybenzene-1,3-dicarboxylic acid (1.00 g, 5.50 mmol). **3** was as isolated as light-brown solid after recrystallization from acetonitrile (1.36 g, 76% yield). ^{1}H NMR (80 MHz, DMSO-d_6) δ 10.13 (1 H, s), 8.48 (1 H, d, J = 1.7 Hz), 7.88-7.44 (6 H, m), 7.24 (4 H, dt, J = 6.0, 3.5 Hz).

2,2'-(oxybis(4,1-phenylene))bis(1*H*-benzo[*d*]imidazole) (4) Synthesized as described for **1**, from 1,2-diaminobenzene (0.85 g, 7.80 mmol) and 4,4′-dicarboxydiphenyl ether (1.00 g, 3.90 mmol). **4** was as isolated as light-brown solid after recrystallization from acetonitrile (0.98 g , 63% yield). ^{1}H NMR (80 MHz, DMSO-d_6) δ 12.85 (2 H, s), 8.25 (4 H, d, J = 8.3 Hz), 7.60 (4 H, dd, J = 6.0, 3.3 Hz), 7.24 (8 H, dd, J = 9.0, 6.4 Hz).

2,2'-((perfluoropropane-2,2-diyl)bis(4,1-phenylene))bis(1*H*-benzo[*d*]imidazole) (5) Synthesized as described for **1**, from 1,2-diaminobenzene (0.55 g, 5.10 mmol) and 4′-(hexafluoroisopropylidene)bis(benzoic acid) (1.00 g, 2.55 mmol). **5** was as isolated as a light-

brown solid after recrystallization from acetonitrile (1.07 g , 78% yield). ^{1}H NMR (80 MHz, DMSO-d_6) δ 8.32 (4 H, d, J = 8.2 Hz), 7.64 (8 H, td, J = 7.1, 3.8 Hz), 7.25 (4 H, dd, J = 6.8, 3.2 Hz).

2.3 Test methodology, sampling and characterization

Stock solutions of aqueous KOD were prepared by diluting the commercial 40 wt.% KOD to 25 wt.% with D_2O. Samples were prepared by dissolving the model compounds (10 mM) in 2 g of MeOD and 8 g of 25 wt.% KOD in 50 mL polytetrafluoroethylene (PTFE) test tubes. The mass fraction of KOD in the mixture was 20 wt.% (corresponding to 4.9 M at 20 °C). The resulting solutions were then purged with argon, sealed, and placed in an oven at 80 °C. The experiment started after equilibrating the samples in the oven for 24 h. Sampling was carried out periodically by taking out 0.75 mL of the liquid after cooling to room temperature. The tubes were thereafter sealed and put back into the oven, and kept under air atmosphere after the first sampling. The samples were analyzed by ^{1}H NMR spectroscopy (0.65 mL) using a Magritek Spinsolve 80 spectrometer operating at 80 MHz and by liquid chromatography (LC) (0.1 mL) using a S2 Waters AQUITY RP-UPLC system equipped with a diode array UV detector coupled to a SQD mass spectrometer (MS). After completion of the test, the organic residuals were collected from the PTFE tubes and analyzed by ^{1}H NMR.

2.4 Computational methods

All density functional theory (DFT) calculations were performed using B3LYP functional[32] and 6-311++G(d, p) basis sets as implemented in Q-Chem 5.2[33] for both optimized geometries and calculated energies. The threshold for the maximum gradient and the self-consistent field (SCF)

energy change between consecutive optimization cycles was 3.0×10^{-3} Hartree/Bohr and 1×10^{-8} Hartree, respectively. The geometry optimizations for intermediate and transition states were carried out in the gas phase. A freezing string method (FSM)[34,35] was used to approximate the reaction path connecting each intermediate state pair. The highest energy point on the reaction path was taken as the first approximation for a transition state. The refined transition state was found by using Baker's partitioned rational-function optimization (P-RFO) algorithm[36] implemented in Q-chem 5.2. Each transition state was verified to connect the designated reactant and product by performing an intrinsic reaction coordinate (IRC)[37] calculation. The vibrational frequencies were calculated to confirm the local minima on the potential energy surface with no imaginary frequencies for all intermediates and one single imaginary frequency for all transition states. Single point energies were computed with the conductor-like polarization continuum model (C-PCM)[38–40] based on the optimized gas-phase geometries. A relative dielectric constant of 78.39 with reference to the bulk water was used to include the effect of the surrounding water medium. Reaction free energy and free energy barrier were calculated at T = 80 °C and 1 atm, the same as the experimental conditions. The free energy (G) of the model compound is the calculated DFT energy (E_{DFT}), including zero-point energy (ZPE), enthalpy contribution ($H = H_{vibration} + H_{rotation} + H_{translation}$), and entropy contribution ($S = S_{vibration} + S_{rotation} + S_{translation}$). Considering that the reaction begins with reactants A and B, goes through transition start TS and results in product C ($A + B \rightarrow TS \rightarrow C$), the reaction free energy and free energy barrier in the solution phase are, for example, given as follows:

$$\Delta G_{(sol)} = G(C_{(sol)}) - G(A_{(sol)}) - G(B_{(sol)}) = \Delta E_{(sol)} + \Delta ZPE_{(gas)} + \Delta H_{(gas)} - T\Delta S_{(gas)}$$

$$\Delta G^{TS}_{(sol)} = G(TS_{(sol)}) - G(A_{(sol)}) - G(B_{(sol)}) = \Delta E^{TS}_{(sol)} + \Delta ZPE^{TS}_{(gas)} + \Delta H^{TS}_{(gas)} - T\Delta S^{TS}_{(gas)}$$

$\Delta E_{(sol)} = E(C_{(sol)}) - E(A_{(sol)}) - E(B_{(sol)})$

$\Delta E^{TS}_{(sol)} = E(TS_{(sol)}) - E(A_{(sol)}) - E(B_{(sol)})$

$\Delta ZPE_{(gas)} = ZPE(C_{(gas)}) - ZPE(A_{(gas)}) - ZPE(B_{(gas)})$

$\Delta ZPE^{TS}_{(gas)} = ZPE(TS_{(gas)}) - ZPE(A_{(gas)}) - ZPE(B_{(gas)})$

$\Delta H_{(gas)} = H(C_{(gas)}) - H(A_{(gas)}) - H(B_{(gas)})$

$\Delta H^{TS}_{(gas)} = H(TS_{(gas)}) - H(A_{(gas)}) - H(B_{(gas)})$

$\Delta S_{(gas)} = S(C_{(gas)}) - S(A_{(gas)}) - S(B_{(gas)})$

$\Delta S^{TS}_{(gas)} = S(TS_{(gas)}) - S(A_{(gas)}) - S(B_{(gas)})$

Here, $\Delta G_{(sol)}$ and $\Delta G^{TS}_{(sol)}$ are the reaction free energy and free energy barrier in the solution phase. E(X(sol)) is the single point energy of species X (where X = A, B, C, TS) computed with the presence of the implicit solvation based on the optimized gas-phase geometry. ZPE, H, and S are calculated in the gas phase based on the optimized gas-phase geometry. The vibration calculations assume harmonic approximation.

For the reaction step involving the hydroxide ion, the hydroxide ion concentration (or pH) was considered in the reaction free energy and free energy barrier. The reaction free energy and free energy barrier as a function of hydroxide ion concentration (or pH) are, for example, calculated as follows:

$A + OH^- \rightarrow TS \rightarrow C$

$\Delta G([OH^-]) = \Delta G_{(sol)} - RT\ln[OH^-] = \Delta G_{(sol)} - 2.303RT(pH - pK_w)$

$$\Delta G^{TS}([OH^-]) = \Delta G^{TS}_{(sol)} - RT\ln[OH^-] = \Delta G^{TS}_{(sol)} - 2.303RT(pH - pK_w)$$

$$\Delta G_{(sol)} = G(C_{(sol)}) - G(A_{(sol)}) - G(OH^-_{(sol)})$$

$$\Delta G^{TS}_{(sol)} = G(TS_{(sol)}) - G(A_{(sol)}) - G(OH^-_{(sol)})$$

Here, pK_w = 12.46, is the acid dissociation constant of water at T = 80 °C,[41] R is the gas constant, and T is the temperature (K). The square brackets indicate the concentration of hydroxide ion (in M). It should be noted that ΔG(sol) and ΔGTS(sol) is the reaction free energy and free reaction energy at a standard concentration in the solution phase where [A] = [OH–] = [C] = 1 M (pH = pK_w = 12.46).

3 RESULTS AND DISCUSSION

3.1 Model system description

A series of arylene-linked bis-benzimidazoles derived from activated and deactivated dicarboxylic acids was defined, as shown in Scheme 2. The model compounds were synthesized by homogeneous condensation reactions between 1,2-diaminobenzene and the corresponding dicarboxylic acids using phosphoric acid as solvent,[42] in line with the common synthetic procedures of polybenzimidazoles.[1] The synthetic procedure was optimized for **1**, which was obtained in 90% yield. The procedure was used without modification for the synthesis **2**-**5**, with yields ranging from 63-85%. After purification by recrystallization, the structural identity of the model compounds was confirmed by ^{1}H NMR (Figure S1) and LC-MS (Figure S2).

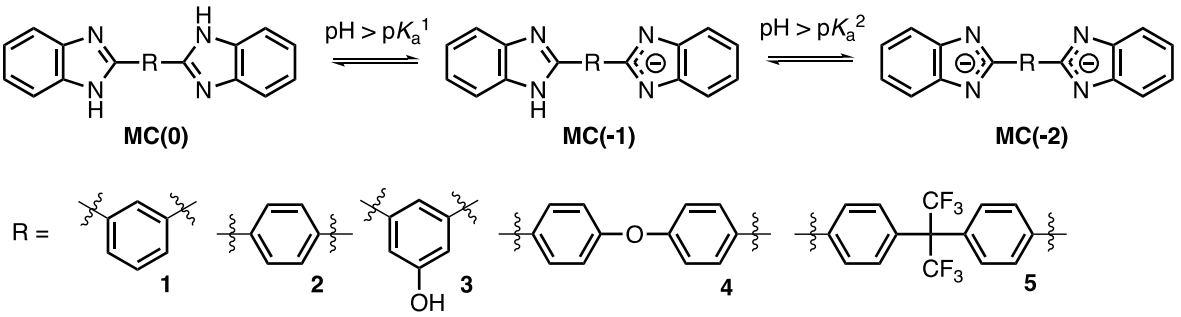

Scheme 2. Chemical structures and acid-base equilibrium of the investigated arylene-linked bis-benzimidazole model compounds derived from moderately activated dicarboxylic acids (**1** and **2**), activated dicarboxylic acids (**3** and **4**) and a deactivated dicarboxylic acid (**5**). Hydroxide ions, counter cations and water molecules are omitted for clarity.

Compound **1** represents the structural repeat unit of the most commonly used and well-characterized polybenzimidazole derivative, i.e. poly(2,2′-*m*-phenylene-bibenzimidazole) (*m*-PBI).[8,28,31,43,44] The para-linked analogue **2** represents the structural repeat unit of poly(2,2′-*p*-phenylene-bibenzimidazole) (*p*-PBI), which is well-known in the high-temperature polymer electrolyte membrane community and extensively characterized in an acidic environment.[45] Similarly, the activated model compounds **3** and **4** and the deactivated compound **5** represent the structural repeat unit of other polybenzimidazole chemistries that have been reported repeatedly in the scientific literature in different technological contexts.[11,46,47]

The pK_a of the corresponding acid of benzimidazole (i.e. the pK_{aH} value) and the pK_a value corresponding to the deprotonation of the neutral benzimidazole have been experimentally determined to 5.6 and 12.8, respectively.[48] It implies that the protonated benzimidazolium ion (structure i, Scheme 1) predominates even in relatively weak Brønsted acids in aqueous solution, while the benzimidazolide ion (structure ii, Scheme 1) predominates at hydroxide concentrations beyond 0.6 M. At the polymer level, it has been found that significantly higher hydroxide

concentrations (3-4 M) are required to reach high degrees of ionization of the *m*-phenylene linked polybenzimidazole.[8]

As pointed out by Patniboon and Hansen,[27] the C2 position of neutral benzimidazole is more electropositive than that of the C2 position of the benzimidazolide form. The neutral form is therefore more susceptible to nucleophilic attack. Thus, in order to aid the interpretation of the results from the degradation study, the pK_a values corresponding to the first and second deprotonation steps as shown in Scheme 2 were calculated and summarized in Table 1. The pK_a calculations were carried out with the PCM implicit solvation without explicit water molecules. It should be noted that compound **3** contains a phenolic proton, and the initial deprotonation to form the corresponding phenoxide anion is denoted as pK_a^0. More calculation details related to pK_a and the deprotonation reactions can be found in Section S2, supporting information. The model compounds at different deprotonation stages are hereafter referred to as MC(0), MC(-1) and MC(-2), where MC refers to the model compounds in general terms or a specific model compound if MC is replaced with an integer. The number in parenthesis refers to the formal charge, as shown in Scheme 2.

Table 1. Calculated pK_a values for the considered model compounds at T = 80 °C.

Model compound #	**pK_a^0**	**pK_a^1**	**pK_a^2**
1	-	12.86	13.26
2	-	13.35	13.65
3	11.73	13.97	15.09
4	-	13.15	13.55
5	-	12.59	12.97

3.2 Stability test

The stability test was carried out by individually dissolving the model compounds in a 20 wt.% (4.9 M at 20 ºC) KOD/D_2O/MeOD solution in PTFE test tubes at a concentration of 10 mM. While compound **3** readily dissolved in KOH/D_2O solution, MeOD was introduced in all samples to support dissolution of **1**, **2**, and **4**. Compound **5** was only partly soluble in the test solution, even after MeOD addition, and the test was therefore carried out semi-heterogeneously. The tests tubes were sealed and kept in an oven at 80 ºC and periodic sampling was carried out for ^{1}H NMR and LC-UV/MS analysis. Some of the signals in the ^{1}H NMR spectra overlapped, which resulted in complex multiplets.

Figure 1a summarizes the ^{1}H NMR evolution in the test period 0-3168 h for compound **1**. Degradation modes leading to the formation of new species would lead to the development of new signals and changed peak integral ratios, but apart from a slightly reduced peak intensity due to partial methanol evaporation and slightly reduced solubility the spectrum of **1** after 3168 h in the test tube appeared nearly identical to that of the starting material. As shown in Figure 1b, this seems supported by the nearly unchanged peak integrals for signal 2-4 relative to signal 1 (defined as 4.00 as this was expected to change the least). The LC measurements of **1** with UV detection showed that the retention characteristics and the shape of the chromatogram remained unchanged during the initial 1104 h of testing. After 2136 and 3168 h, the MS data revealed a signal with a m/z ratio of 239.46 in the small new peak that appeared, corresponding to the structure of **1** where one of the benzimidazole substituents is replaced with a carboxylic acid moiety (see Figure S3a). This may also be the reason for the changed appearance of the chromatogram although the

concentration was likely too low to change the appearance of the ^{1}H NMR spectrum and the integral ratios.

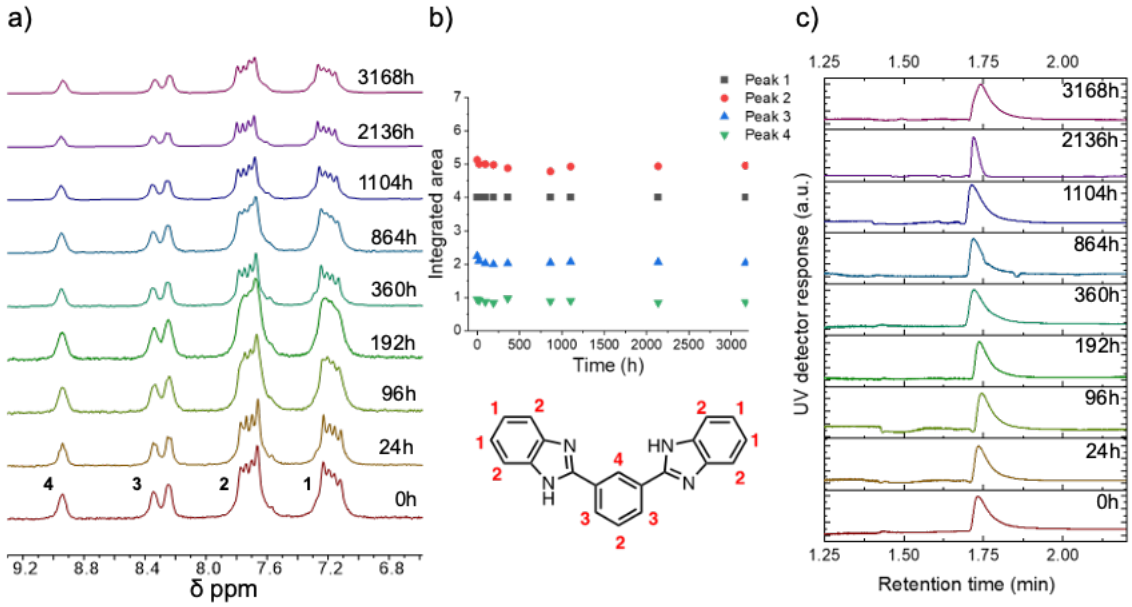

Figure 1. ^{1}H NMR evolution (a) and peak integrals (b) and LC-UV (c) of **1** during aging in 20 wt.% KOD in D_2O/MeOD at 80 ºC for up to 3168 h. The peak integral for the signal assigned to proton 1 is defined as 4.00, and the other peak integrals are given relative to that.

As shown in Figure 2a, the ^{1}H NMR spectrum of compound **2** was nearly unchanged during the initial 2136 h of the stability test. The disappearance of the ^{1}H NMR signals in the aromatic region after 3168 h coincided with the disappearance of the MeOD residual solvent peak at around 3.5 ppm (not shown). The latter was likely due to evaporative loss of MeOD, which resulted in partial precipitation and a semi-heterogenous system in the later phase of the test. The LC-UV data followed the same trend as observed for **1**. A peak with m/z ratio of 311.49 was observed in the main elution peak, in good agreement with the expected molecular mass of **2**. As for compound **1**,

a new peak was observed in the MS data of **2** after 3168 h with a m/z ratio corresponding well with the mono-hydrolyzed compound (Figure S3b).

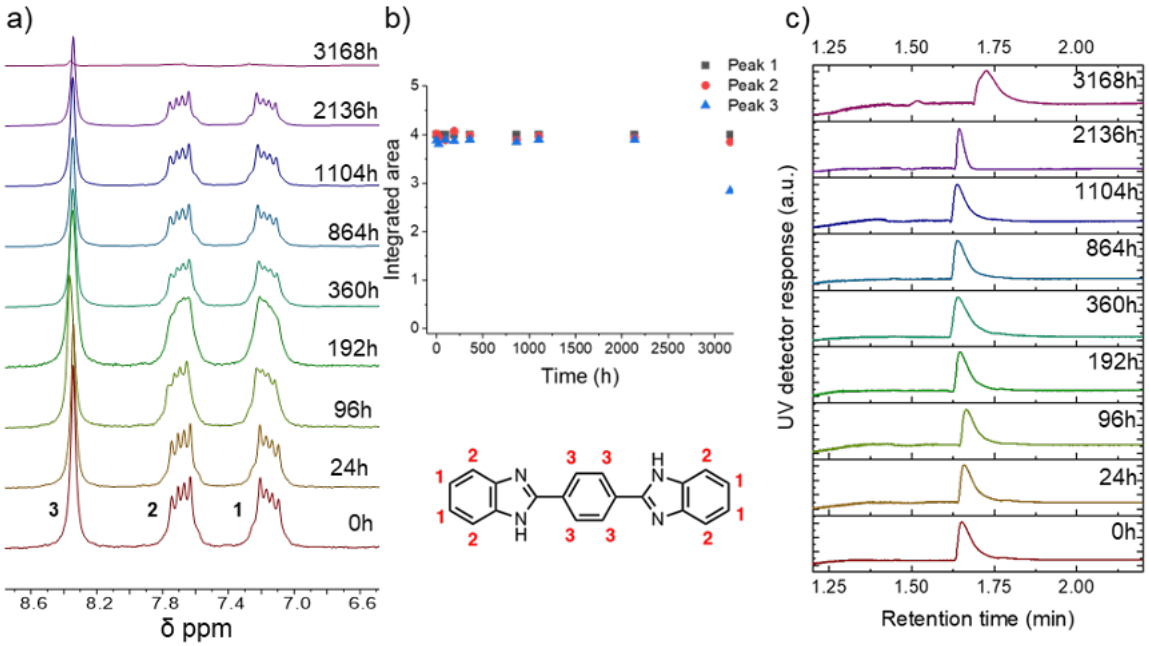

Figure 2. ^{1}H NMR evolution (a), peak integrals (b) and LC-UV (c) of **2** during aging in 20 wt.% KOD in D_2O/MeOD at 80 ºC for up to 3168 h. The peak integral for the signal assigned to proton 1 is defined as 4.00, and the other peak integrals are given relative to that.

The ^{1}H NMR evolution of compound **3** is summarized in Figure 3a. One obvious observation is the gradual decay of the peaks at 7.5 and 8.1 ppm, which is due to deuterium exchange at position 3 and 2´, respectively. The deuterium exchange was also confirmed by the LC-MS data, as shown by the increase of the intensity of the signals for m/z 328 and 329 relative to m/z 327 in Figure S4. Deuterium exchange has also been observed previously in model system studies of organic cations in KOD solution.[23] The ^{1}H NMR signal originating from the protons adjacent to the hydroxyl function partly overlapped with the signal from the aromatic protons at the benzimidazole groups, and the signals were therefore integrated together as peak 2. The apparent decay of the integrals

for peak 2 and 3 in Figure 3b is thus a result of the deuterium exchange. The LC-UV data did not reveal any development of additional peaks during the first 2136 h of the test. The MS data did not show any presence of the C2-cleaved decomposition product.

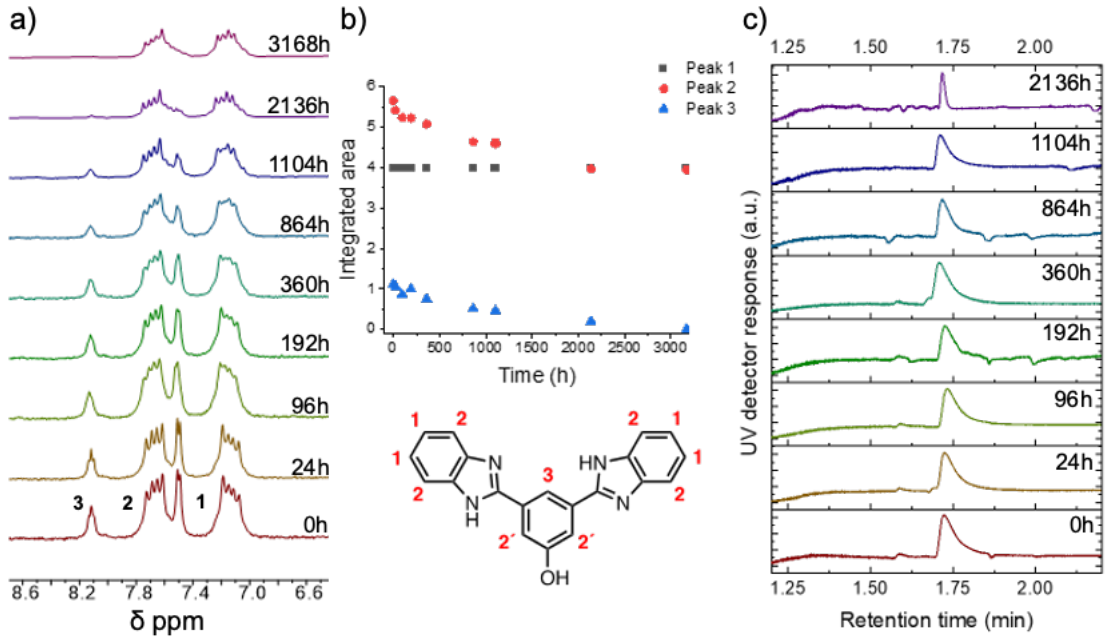

Figure 3. ^{1}H NMR evolution (a), peak integrals (b) and LC-UV (c) of 3 during aging in 20 wt.% KOD in D_2O/MeOD at 80 ºC for up to 3168 h. The peak integral for the signal assigned to proton 1 is defined as 4.00, and the other peak integrals are given relative to that.

As shown in Figure 4a, the ^{1}H NMR data for compound **4** were nearly unchanged during the first 192 h of the test. Figure 4b shows that the integrals for peak 2 and 3 started to increase after 360 h, which is an artifact resulting from deuterium exchange at position 1. The deuterium exchange was supported by the MS data, as shown in Figure S5 by the gradually increasing signal intensity for m/z 404.7 and 405.7. The C2-cleaved decomposition product with one of the benzimidazole groups replaced by a carboxylate function could be identified from the MS data in the tail of the

main elution peak after 864 h at m/z 331 and could be seen in the elution peak tail until the end of the test (Figure S3c).

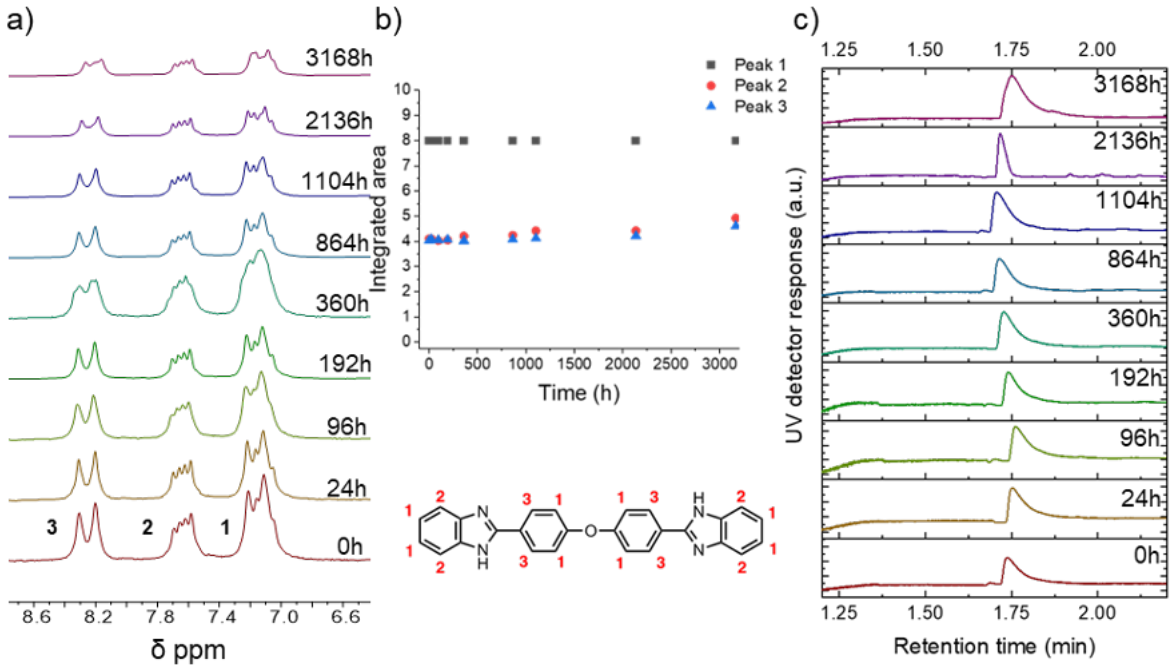

Figure 4. ^{1}H NMR evolution (a), peak integrals (b) and LC-UV (c) of **4** during aging in 20 wt.% KOD in D_2O/MeOD at 80 ºC for up to 3168 h. The peak integral for the signal assigned to proton 1 is defined as 8.00, and the other peak integrals are given relative to that.

Compound **5** was considerably less soluble in the test solution than compound **1**-**4**, and was therefore tested in a semi-heterogenous manner with some solid residuals at the bottom of the PTFE tube. As a result, the concentration of **5** in the test solution was lower than for compound **1**-**4**. As shown in Figure 5a, the ^{1}H NMR spectra remained nearly unchanged during the initial 1104 h. This is also supported by the nearly unchanged peak integrals in this time interval as shown in Figure 5b. After 2136 h, the ^{1}H NMR signal intensity was significantly reduced and continued to decrease after that, likely due to evaporative loss of MeOD which resulted in reduced solubility.

The LC-UV data, as summarized in Figure 5c, showed a single elution peak with a shape that did not change during the initial 1104 h. After 360 h, the MS data confirmed the presence of the decomposition product with one of the benzimidazoles replaced by a carboxylate function in the tail of the main elution peak. The low intensity of the main elution peak in the LC-UV data after 3168 h confirms the low concentration of **5** in the test solution, but the MS data clearly showed the presence of a degradation product with a m/z ratio of 465.5 (Figure S3d).

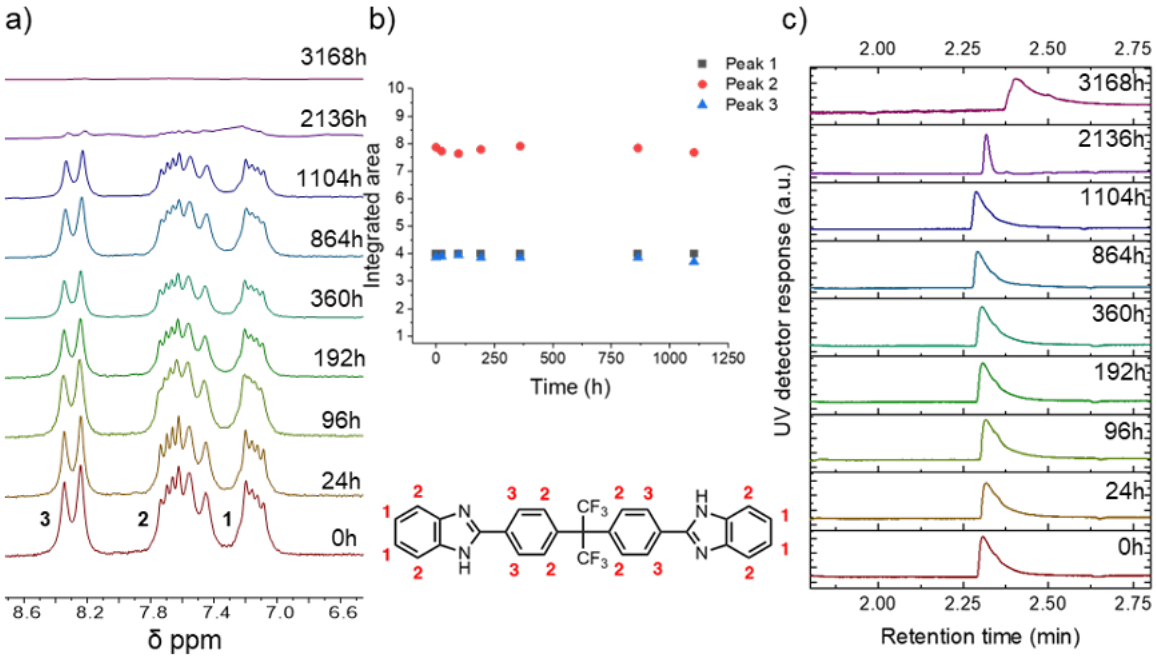

Figure 5. ^{1}H NMR evolution (a), peak integrals (b) and LC-UV (c) of **5** during aging in 20 wt.% KOD in D_2O/MeOD at 80 ºC for up to 3168 h. The peak integral for the signal assigned to proton 1 is defined as 4.00, and the other peak integrals are given relative to that.

Due to limited solubility or insufficient chemical stability in the test solution, a suitable internal standard for product quantification by ^{1}H NMR could not be identified. However, a qualitative ranking was made based on the obtained MS data by considering elapsed time until degradation products were first detected. As can be seen in Figure S3, the degradation products in the form of

the mono-hydrolyzed compound were detected for compounds **1**, **2**, **4**, and **5** after 2136, 3168, 864, and 360 h respectively. As for **3**, the MS data did not show any signs of degradation throughout the whole period. This aligns well with the expectations for the presence of an electron donating group in the molecule, which should lower the electropositivity of the C2. With an electron-withdrawing group, on the contrary, the electropositivity of the C2 position is expected to increase and accelerate degradation. This argumentation is aligned with the experimental results for compound **5**, where the degradation product was identified first. What was surprising, however, is that compound **4** saw degradation after only 864 h despite bearing an electron donating ether linkage. Both **1** and **2** proved excellent stability, with **2** being the latest to show the presence of the degradation product. For compound **3**, no degradation product could be observed during the experiment. Based on the experimental data it can thus be concluded that the relative stability increased in the order of **5** < **4** < **1** ≈ **2** < **3** in the 20 wt.% KOD/D_2O/MeOD solution. Previous mechanistic degradation studies on quaternary ammonium functionalized polymers show that the presence of molecular oxygen results in faster degradation of the cationic head groups and generation of active oxygen species that trigger backbone degradation.[49] The identification of hydrolysis as the main degradation mode in the present work indicate that molecular oxygen was not involved in the predominating degradation pathway. The low oxygen solubility in concentrated KOD could be one of the reasons for this observation.

3.3 Computational insight into the degradation mechanism

The postulated degradation mechanism of bis-benzimidazole derivatives in alkaline solution is illustrated in Scheme 3.[27] The degradation is triggered by the hydroxide attack at the carbon atom

in C2 position, followed by ring-opening, amide hydrolysis, and complete chain scission, resulting in free diamine and a carboxylate-containing benzimidazole derivative as degradation products.

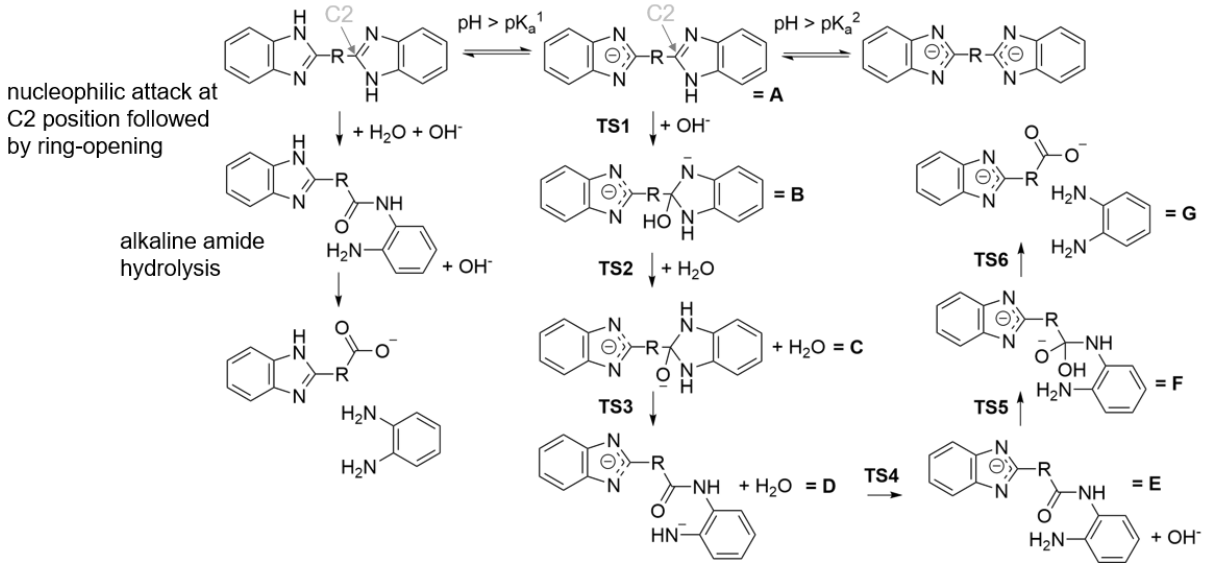

Scheme 3. Postulated degradation mechanism of arylene-linked bis-benzimidazoles in an alkaline environment.[27]

In an alkaline solution, the model compounds are present at different degrees of ionization, as shown in Scheme 2 and Table 1. The mole fraction of the model compounds present at different degrees of ionization calculated based on the pK_a values in Table 1 are shown in Figure 6a, where the neutral model compound is denoted as MC(0). The model compounds with one and two protons deprotonated are denoted MC(-1), and MC(-2), respectively. More calculation details related to the model fraction can be found in Section S2, supporting information. The mole fraction of the model compounds present at different degrees of ionization calculated based on the pK_a values in Table 1 are shown in Figure 6a. The data were obtained from the thermodynamic cycle shown in Figure S6 and the free reaction energies for deprotonation as summarized in Table S1. As the KOH

concentration increases and the equilibria shown in Scheme 2 and Figure S7 are shifted to the right, the mole fraction of the neutral compounds decreases. The degree of ionization can be approximated as **3** > **5** > **1** > **4** > **2**. In 20 wt.% KOH, the predominating form of model compound **5** is **5**(-2), while the MC(-1) form predominates for model compound **1** and **3**. In the case of model compound **2** and **4**, MC(0), i.e. the neutral form, is the predominating form. It should be noted that the phenolic proton in model compound **3** is more likely to deprotonate than the others. Thus, **3**(-1) is in the phenoxide anion and **3**(-2) refers to the phenoxide form with one of the benzimidazoles deprotonated. The degree of imidazole deprotonation is **5** > **1** > **4** > **2** > **3**.

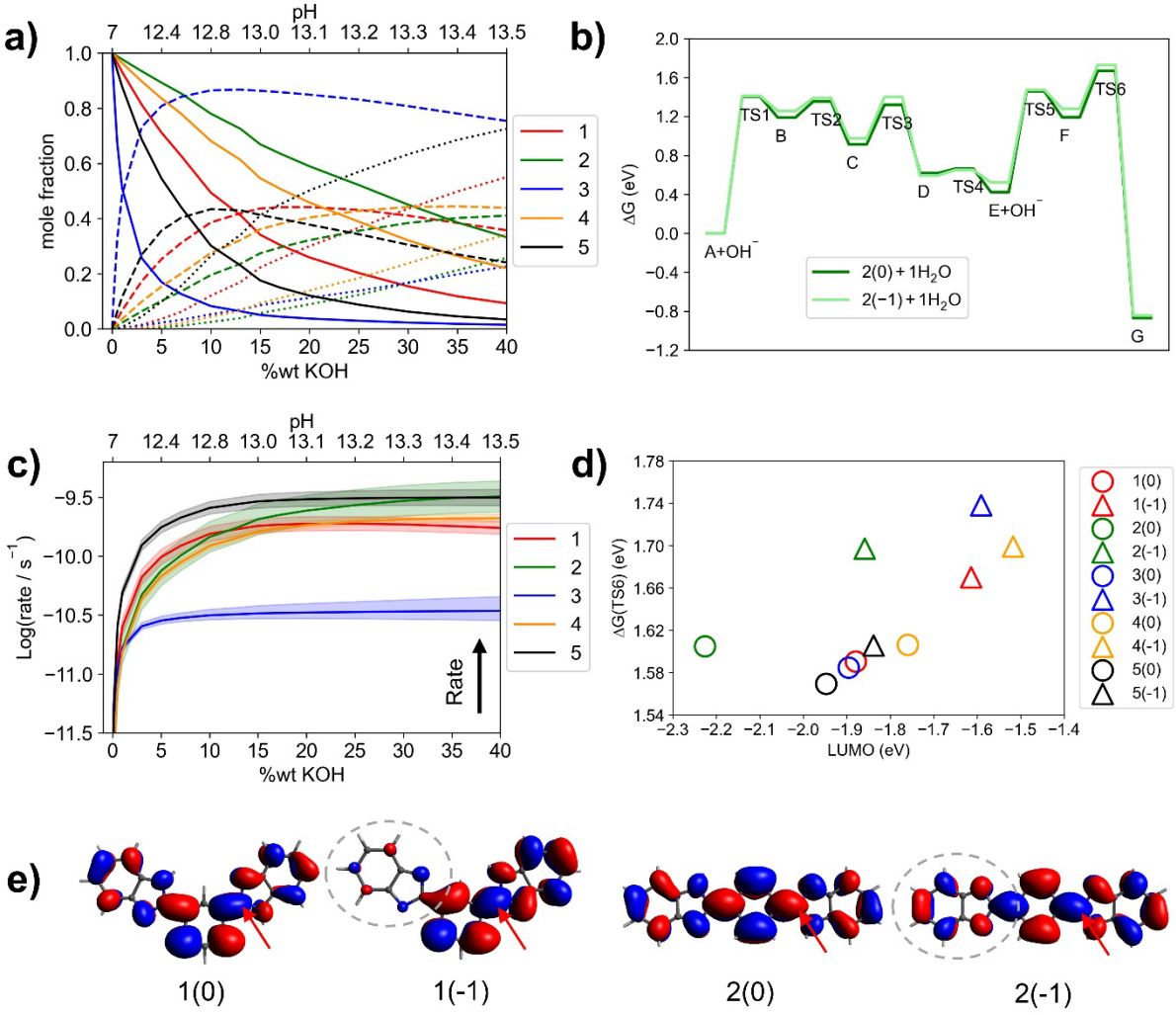

Figure 6. a) Mole fraction of different deprotonation states as a function of KOH concentration. The mole fraction of the model compound in the MC(0), MC(-1) and MC(-2) forms is indicated by solid, dashed, and dotted lines, respectively. b) Reaction energy profile following the proposed degradation mechanism in Scheme 3 for model compound **2** with one explicit water molecule at T = 80 °C and pH = 12.46. c) Approximated degradation rate as a function of KOH concentrations at T = 80 °C. d) Effective energy barrier; ΔG(TS6) vs. LUMO energy of the model compounds. The calculated effective energy barriers and LUMO energy are averaged from the calculations with two and three explicit water molecules. e) LUMO isosurface: **1**(0), **1**(-1), **2**(0), **2**(-1). The red arrows point to the C2 position where the degradation occurs and the grey circles indicate the deprotonated side.

DFT calculations were carried out to investigate the free energy profile along the assumed degradation pathway as shown in Scheme 3. Since the degradation occurs in an aqueous alkaline environment, the solvent effect was considered. A previous theoretical study has shown that combining explicit water molecules with implicit solvation gives a good agreement between the experimental and the DFT-predicted energy barrier for the degradation of *m*-PBI in alkaline solution.[27] Thus, water molecules were explicitly placed near the model compound structure along the degradation pathway in this study. More calculation details related to the implicit-explicit solvation model used in the calculations can be found in Section S4, supporting information.

For the first hydroxide ion attack at the C2 position, the free reaction energy for MC(-2) exceed 2.00 eV for model compound **1**, **2**, **4**, and **5**, which is considerably higher than for a fraction of MC(0) and MC(-1) present in the solution (Table S2). For model compound **3**(-2), the energy barrier for the first hydroxide ion attack is comparable to that of **3**(-1), but according to the pK_a

value, the mole fraction of **3**(-2) in solution is low compared to the **3**(0) and **3**(-1) forms. On this background, it is most likely that the degradation proceeds from the MC(0) and MC(-1) forms, and the full reaction path from MC(-2) is therefore not considered. Since the degradation occurs in an aqueous alkaline environment, the combination of implicit and explicit solvation models was used to consider the solvent effect. The configurations of explicit water for MC(0) and MC(-1) are shown in Figure S8 and S9, respectively, and more calculation details related to the implicit-explicit solvation model used in the calculations can be found in Section S4, supporting information.

Figure 6b shows the free energy profile following the postulated degradation mechanism of model compound **2**. For the other model compounds, the free energy profiles at different degrees of deprotonation and solvation are shown in Figure S10-S12 and the effective energy barriers are summarized in Figure S13. It can be seen that the highest transition state along the postulated degradation mechanism for all MC(0) and MC(-1) model compounds is TS6, relating to the amide cleavage during the chain scission. Thus, the effective energy barrier, which determines the degradation rate is the free energy difference between TS6 and the initial reactant state ($A+OH^-$). Furthermore, the effective energy barrier is found to be lower as the KOH concentration increases.[27]

Besides the C2-cleavage products observed in our experiments, deuterium exchange was observed for model compound **3** and **4**. The free reaction energies for the deuterium exchange reaction at the aromatic ring according to the reactions shown in Figure S14 are summarized in Table S3. It is assumed that the hydrogen atoms in the model compound structure exchange with deuterium from the surrounding solution. The predicted deuterium exchange positions are in agreement with experimental data for model compound **3** and **4**. It is important to stress that the

free energy profile along the degradation pathway (Figure S15**)** and the pK_a value for model compounds **3** and **4 (**Table S4**)** are unaffected by the deuterium exchange.

Figure 6c shows the estimated degradation rate as a function of KOH concentration. The degradation rate is calculated by including the contribution from the MC(0) and MC(-1) forms of each model compound. As justified above, it is assumed that the contribution from the MC(-2) state is negligible as it is unlikely to degrade due to the high energy barrier for the initial nucleophilic attack and the low concentration relative to the other forms. The degradation rates are calculated from the average effective energy barrier with two and three explicit water molecules. The shaded areas indicate the uncertainty of the degradation rate c, which is calculated from the standard error of the average effective energy barriers with two and three explicit water molecules. More calculation details about the degradation rate can be found in section S6, supporting information. At 20 wt.% KOH, the following order of degradation rate is calculated: **5** > **2** ≈ **4** ≈ **1** > **3**. This suggests that model compound **5** has the lowest alkaline stability compared to the others, while model compound **3** is the most stable in the alkaline solution, which is in good agreement with the experimental results. At 20 wt% KOH, the degradation rate for the model compounds **1**, **2**, and **4** are found to be similar within the uncertainty.

Figure S16 shows contributions to the degradation rate from the MC(0) and MC(-1) fractions. The degradation rate of model compound **1-4** is mainly from the MC(0). On the other hand, for **5**, both **5**(0) and **5**(-1) contribute to the degradation rate. It is found that the energy difference in the effective energy barrier between the MC(0) and MC(-1) state is about 0.08, 0.09, 0.15, and 0.09 eV for **1**, **2**, **3** and **4**, respectively. The difference is only 0.04 eV for **5**, and therefore both **5**(0) and **5**(-1) contribute to the overall degradation rate.

The difference in effective energy barrier of the main contributing species between model compound **1**, **3,** and **5** is within 0.01 eV, as shown in Figure S17b. A significant difference in the degradation rate between these three model compounds is due to the difference in the mole fraction of the main contributing species. As given in Figure S17a and S17c, the degradation rate and the mole fraction of the main contributing species is in the following order: **3**(0) < **1**(0) < **5**(0) + **5**(-1). For **2**, **4**, and **5**, even though the mole fraction of the main contributing species solution is comparable, the effective energy barrier of the main contributing species of **2** and **4** is higher than that of **5** . Therefore, the degradation rate of **2** and **4** is higher than that of **5**.

It is important to note that the effective energy barrier was approximated with specific static configurations and a limited amount of explicit water molecules around the model compound structure. Recently, Wu et al.[50] have investigated the distribution of water molecules and hydroxide ions around imidazolium-based molecules by molecular dynamic (MD) simulation with about 100-400 explicit water molecules. They have found significantly different distribution around the different imidazolium structures due to the modification with various substitutions at the same hydration level. Also, it has been suggested that the alkaline stability of the imidazolium cation strongly depends on the hydration level, i.e. the number of water molecules per cationic group,[51,52] which also significantly depends on the operating conditions at the device level.[53] In our study, further increasing the number of explicit water molecules to complete the hydration shell for each model compound along the degradation by performing MD simulation would be required to achieve higher accuracy. However, such a simulation requires significantly more computational time and is considered beyond the scope of the present work.

To further understand the structural and electronic effects of the considered model compounds on their alkaline stability, the atomic charge on each model compound was considered

as shown in Figure S18. For neutral molecules, i.e. MC(0), the natural bond order (NBO) analysis[54] shows that the carbon atoms at the C2 position carry the highest positive charge. After deprotonation, the atomic charge on the C2 position becomes slightly negative. Similar atomic charges were found for all considered model compounds at the C2 position, and the differences in stability can thus not solely be explained by differences in atomic charge. Previous studies, which mostly focused on the alkaline stability of imidazolium cations, suggest that the lowest unoccupied molecular orbital (LUMO) energies of imidazolium cations correlate with their alkaline stability.[55–57] The imidazolium-based cations are positively charged and highly electrophilic, and those having a lower LUMO energy are more vulnerable to hydroxide ions.

The LUMO energy level as a function of the effective energy barrier for degradation and the LUMO isosurface for the model compounds in the present work are shown in Figure 6d-e and in Figure S19-S21. Generally, the energy barrier for the rate-determining degradation step increases with increasing LUMO level. It can, however, be seen that model compound **2**(0), **2**(-1), and **3**(-1) deviate from this trend. As shown in Figure S19, the LUMO isosurface distributes evenly over the model compound structure, including in the C2 position for all considered model compounds in the MC(0) form. After the first deprotonation, i.e., for the compounds in the MC(-1) form, the LUMO level always increases. For model compounds **1**, **4,** and **5**, the LUMO isosurface has mainly weight near the non-deprotonated side, including the C2 position where the degradation is most likely to occur. For model compound **2** and **3** in the MC(-1) form, which showed the highest alkali stability in the experimental study, the LUMO isosurface distributes all over the structure, including the C2 position on both sides. However, the LUMO level alone is not necessarily an accurate single descriptor for the alkaline stability of benzimidazoles and benzimidazolides in an alkaline environment because the fractions of model compounds are

determined by their pK_a. For example, the high stability of compound **3** can be attributed to the low value of pK_a^0, resulting in a low concentration of **3**(0), while the effective barrier to the degradation of the most dominant fraction **3**(-1) is the highest (1.74 eV) among the model compounds. In contrast, the least stable compound **5**, has relatively low pK_a values for the first and second deprotonation steps, but also low effective barriers for degradation of both **5**(0) and **5**(-1).

CONCLUSIONS

A series of arylene-linked bis-benzimidazoles was synthesized and kept in concentrated KOD solutions at 80 °C, and the chemical changes were monitored by ^{1}H NMR and LC-UV/MS. The highly activated model equipped with a phenol functionality on the linking arylene showed best stability and no signs of degradation apart from deuterium exchange, whereas the strongly deactivated bis-benzimidazole with a hexafluoroisoproylidene link degraded fastest. DFT calculations support that the degradation mainly proceeds via the fraction of neutral benzimidazole units, and the stability can therefore be improved by increasing the degree of deprotonation along the molecule and thereby lowering the electropositivity at the C2 position.

Supporting Information. ^{1}H NMR and mass spectra of model compounds; Free reaction energy for deprotonation of model compounds; Reaction energy profiles for proposed degradation pathways; Free reaction energy for deuterium exchange; Approximation of degradation rates

Corresponding Author

* Corresponding author: David Aili (e-mail: larda@dtu.dk)

Author Contributions

The manuscript was written through contributions of all authors. All authors have given approval to the final version of the manuscript. ‡These authors contributed equally.

ACKNOWLEDGMENT

This work was financially supported by Innovation Fund Denmark (DREAME, 9067-00055B).

REFERENCES

(1) Aili, D.; Yang, J.; Jankova, K.; Henkensmeier, D.; Li, Q. From polybenzimidazoles to polybenzimidazoliums and polybenzimidazolides. *J. Mater. Chem. A*. **2020**, *8*, 12854-12886.

(2) Aili, D.; Henkensmeier, D.; Martin, S.; Singh, B.; Hu, Y.; Jensen, J. O.; Cleemann, L. N.; Li, Q. New insight and recent progress of polybenzimidazole based high temperature polymer electrolyte membrane fuel cells. *Electrochem. Energy Rev.* **2020**, *3*, 793-845.

(3) Noh, C.; Serhiichuk, D.; Malikah, N.; Kwon, Y.; Henkensmeier, D. Optimizing the performance of meta-polybenzimidazole membranes in vanadium redox flow batteries by adding an alkaline pre-swelling step. *Chem. Eng. J.* **2021**, *407*, 126574.

(4) Kraglund, M. R.; Carmo, M.; Schiller, G.; Ansar, S. A.; Aili, D.; Christensen, E.; Jensen, J. O. Ion-solvating membranes as a new approach towards high rate alkaline electrolyzers. *Energy Environ Sci* **2019**, *12*, 3313-3318.

(5) Trisno, M. L. A.; Dayan, A.; Lee, S. J.; Egert, F.; Gerle, M.; Kraglund, M. R.; Jensen, J. O.; Aili, D.; Roznowska, A.; Michalak, A.; Park, H. S.; Razmjooei, F.; Ansar, S.-A.;

Henkensmeier, D. Reinforced gel-state polybenzimidazole hydrogen separators for alkaline water electrolysis. *Energy Environ. Sci.* **2022**, *15*, 4362-4375.

(6) Zhu, L. X.; Swihart, M. T.; Lin, H. Q. Unprecedented size-sieving ability in polybenzimidazole doped with polyprotic acids for membrane H_2/CO_2 separation. *Energy Environ. Sci* **2018**, *11*, 94-100.

(7) Melchior, J.-P.; Majer, G.; Kreuer, K.-D. Why do proton conducting polybenzimidazole phosphoric acid membranes perform well in high-temperature PEM fuel cells? *Phys. Chem. Chem. Phys.* **2017**, *19*, 601-612.

(8) Aili, D.; Jankova, K.; Han, J.; Bjerrum, N. J.; Jensen, J. O.; Li, Q. Understanding ternary poly(potassium benzimidazolide)-based polymer electrolytes. *Polymer* **2016**, *84*, 304-310.

(9) Thomas, O. D.; Soo, K. J. W. Y.; Peckham, T. J.; Kulkarni, M. P.; Holdcroft, S. Anion conducting poly(dialkyl benzimidazolium) salts. *Polym. Chem.* **2011**, *2*, 1641-1643.

(10) Tang, H.; Aili, D.; Geng, K.; Gao, J.; Li, Q.; Li, N. On the stability of imidazolium and benzimidazolium salts in phosphoric acid based fuel cell electrolytes. *J. Power Sources* **2021**, *515*, 230642.

(11) Henkensmeier, D.; Cho, H. R.; Kim, H. J.; Kirchner, C. N.; Leppin, J.; Dyck, A.; Jang, J. H.; Cho, E.; Nam, S. W.; Lim, T. H. Polybenzimidazolium hydroxides - Structure, stability and degradation. *Polym. Degrad. Stab.* **2012**, *97*, 264-272.

(12) Marino, M. G.; Kreuer, K.-D. Alkaline stability of quaternary ammonium cations for alkaline fuel cell membranes and ionic liquids. *ChemSusChem* **2015**, *8*, 513-523.

(13) You, W.; Hugar, K. M.; Selhorst, R. C.; Treichel, M.; Peltier, C. R.; Noonan, K. J. T.; Coates, G. W. Degradation of organic cations under alkaline conditions. *J. Org. Chem.* **2021**, *86*, 254-263.

(14) Fan, J.; Wright, A. G.; Britton, B.; Weissbach, T.; Skalski, T. J. G.; Ward, J.; Peckham, T. J.; Holdcroft, S. Cationic polyelectrolytes, stable in 10 M KOH_{aq} at 100 °C. *ACS Macro Lett.* **2017**, *6*, 1089-1093.

(15) Yu, N.; Dong, J.; Wang, T.; Jin, Y.; Tang, W.; Yang, J. Two new anion exchange membranes based on poly(bis-arylimidazolium) ionenes blend polybenzimidazole. *Polymer* **2022**, *240*, 124491.

(16) Thomas, O. D.; Soo, K.; Peckham, T. J.; Kulkarni, M. P.; Holdcroft, S. A stable hydroxide-conducting polymer. *J. Am. Chem. Soc.* **2012**, *134*, 10753-10756.

(17) Wright, A. G.; Holdcroft, S. Hydroxide-stable ionenes. *ACS Macro Lett.* **2014**, *3*, 444-447.

(18) Olsson, J. S.; Pham, T. H.; Jannasch, P. Poly(arylene piperidinium) hydroxide ion exchange membranes: Synthesis, alkaline stability, and conductivity. *Adv. Funct. Mater.* **2018**, *28*, 1702758.

(19) Wang, T.; Dong, J.; Yu, N.; Tang, W.; Jin, Y.; Xu, Y.; Yang, J. Synthesis and properties of a new ether-free poly(bis-alkylpiperidinium) polymer for the anion exchange membrane. *Eur. Polym. J.* **2022**, *173*, 111271.

(20) Lee, W. H.; Kim, Y. S.; Bae, C. Robust hydroxide ion conducting poly(biphenyl alkylene)s for alkaline fuel cell membranes. *ACS Macro Lett.* **2015**, *4*, 814-818.

(21) Park, E. J.; Maurya, S.; Hibbs, M. R.; Fujimoto, C. H.; Kreuer, K.-D.; Kim, Y. S. Alkaline stability of quaternized Diels-Alder polyphenylenes. *Macromolecules* **2019**, *52*, 5419-5428.

(22) Wang, L.; Peng, X.; Mustain, W. E.; Varcoe, J. R. Radiation-grafted anion-exchange membranes: The switch from low- to high-density polyethylene leads to remarkably enhanced fuel cell performance. *Energy Environ. Sci.* **2019**, *12*, 1575-1579.

(23) Fan, J. T.; Willdorf-Cohen, S.; Schibli, E. M.; Paula, Z.; Li, W.; Skalski, T. J. G.; Sergeenko, A. T.; Hohenadel, A.; Frisken, B. J.; Magliocca, E.; Mustain, W. E.; Diesendruck, C. E.; Dekel, D. R.; Holdcroft, S. Poly(bis-arylimidazoliums) possessing high hydroxide ion exchange capacity and high alkaline stability. *Nat Commun* **2019**, *10*, 2306.

(24) Sana, B.; Das, A.; Jana, T. Cross-linked polybenzimidazoles as alkaline stable anion exchange membranes. *ACS Appl. Energy Mater.* **2022**, *5*, 3626–3637.

(25) Das, A.; Sana, B.; Bhattacharyya, R.; Chandra Ghosh, P.; Jana, T. Cross-linked alkaline anion exchange membrane from *N*-spirocyclic quaternary ammonium and polybenzimidazole. *ACS Appl. Polym. Mater.* **2022**, *4*, 1523–1534.

(26) Sana, B.; Das, A.; Sharma, M.; Jana, T. Alkaline anion exchange membrane from alkylated polybenzimidazole. *ACS Appl. Energy Mater.* **2021**, *4*, 9792–9805.

(27) Patniboon, T.; Hansen, H. A. Degradation of polybenzimidazole in alkaline solution with first-principles modeling. *Electrochim. Acta* **2021**, *398*. 139329

(28) Aili, D.; Jankova, K.; Li, Q.; Bjerrum, N. J.; Jensen, J. O. The stability of poly(2,2′-(*m*-phenylene)-5,5′-bibenzimidazole) membranes in aqueous potassium hydroxide. *J. Memb. Sci.* **2015**, *492*, 422-429.

(29) Aili, D.; Wright, A. G.; Kraglund, M. R.; Jankova, K.; Holdcroft, S.; Jensen, J. O. Towards a stable ion-solvating polymer electrolyte for advanced alkaline water electrolysis. *J. Mater. Chem. A* **2017**, *5*, 5055-5066.

(30) Hu, B.; Huang, Y.; Liu, L.; Hu, X.; Geng, K.; Ju, Q.; Liu, M.; Bi, J.; Luo, S.; Li, N. A stable ion-solvating PBI electrolyte enabled by sterically bulky naphthalene for alkaline water electrolysis. *J. Memb. Sci.* **2022**, *643*, 120042.

(31) Aili, D.; Hansen, M. K.; Renzaho, R. F.; Li, Q.; Christensen, E.; Jensen, J. O.; Bjerrum, N. J. Heterogeneous anion conducting membranes based on linear and crosslinked KOH doped polybenzimidazole for alkaline water electrolysis. *J. Memb. Sci.* **2013**, *447*, 424-432.

(32) Becke, A. D. A new mixing of Hartree-Fock and local density-functional theories. *J. Chem. Phys.* **1993**, *98*, 1372-1377.

(33) Shao, Y.; Gan, Z.; Epifanovsky, E.; Gilbert, A. T. B.; Wormit, M.; Kussmann, J.; Lange, A. W.; Behn, A.; Deng, J.; Feng, X.; Ghosh, D.; Goldey, M.; Horn, P. R.; Jacobson, L. D.; Kaliman, I.; Khaliullin, R. Z.; Kuš, T.; Landau, A.; Liu, J.; Proynov, E. I.; Rhee, Y. M.; Richard, R. M.; Rohrdanz, M. A.; Steele, R. P.; Sundstrom, E. J.; Woodcock, H. L.; Zimmerman, P. M.; Zuev, D.; Albrecht, B.; Alguire, E.; Austin, B.; Beran, G. J. O.; Bernard, Y. A.; Berquist, E.; Brandhorst, K.; Bravaya, K. B.; Brown, S. T.; Casanova, D.; Chang, C. M.; Chen, Y.; Chien, S. H.; Closser, K. D.; Crittenden, D. L.; Diedenhofen, M.; Distasio, R. A.; Do, H.; Dutoi, A. D.; Edgar, R. G.; Fatehi, S.; Fusti-Molnar, L.; Ghysels, A.; Golubeva-Zadorozhnaya, A.; Gomes, J.; Hanson-Heine, M. W. D.; Harbach, P. H. P.; Hauser, A. W.; Hohenstein, E. G.; Holden, Z. C.; Jagau, T. C.; Ji, H.; Kaduk, B.; Khistyaev, K.; Kim, J.; Kim, J.; King, R. A.; Klunzinger, P.; Kosenkov, D.; Kowalczyk, T.; Krauter, C. M.; Lao, K. U.; Laurent, A. D.; Lawler, K. v.; Levchenko, S. v.; Lin, C. Y.; Liu, F.; Livshits, E.; Lochan, R. C.; Luenser, A.; Manohar, P.; Manzer, S. F.; Mao, S. P.; Mardirossian, N.; Marenich, A. v.; Maurer, S. A.; Mayhall, N. J.; Neuscamman, E.; Oana, C. M.; Olivares-Amaya, R.; Oneill, D. P.; Parkhill, J. A.; Perrine, T. M.; Peverati, R.; Prociuk, A.; Rehn, D. R.; Rosta, E.; Russ, N. J.; Sharada, S. M.; Sharma, S.; Small, D. W.; Sodt, A.; Stein, T.; Stück, D.; Su, Y. C.; Thom, A. J. W.; Tsuchimochi, T.; Vanovschi, V.;

Vogt, L.; Vydrov, O.; Wang, T.; Watson, M. A.; Wenzel, J.; White, A.; Williams, C. F.; Yang, J.; Yeganeh, S.; Yost, S. R.; You, Z. Q.; Zhang, I. Y.; Zhang, X.; Zhao, Y.; Brooks, B. R.; Chan, G. K. L.; Chipman, D. M.; Cramer, C. J.; Goddard, W. A.; Gordon, M. S.; Hehre, W. J.; Klamt, A.; Schaefer, H. F.; Schmidt, M. W.; Sherrill, C. D.; Truhlar, D. G.; Warshel, A.; Xu, X.; Aspuru-Guzik, A.; Baer, R.; Bell, A. T.; Besley, N. A.; Chai, J. da; Dreuw, A.; Dunietz, B. D.; Furlani, T. R.; Gwaltney, S. R.; Hsu, C. P.; Jung, Y.; Kong, J.; Lambrecht, D. S.; Liang, W.; Ochsenfeld, C.; Rassolov, V. A.; Slipchenko, L. v.; Subotnik, J. E.; van Voorhis, T.; Herbert, J. M.; Krylov, A. I.; Gill, P. M. W.; Head-Gordon, M. Advances in molecular quantum chemistry contained in the Q-Chem 4 Program Package. *Mol. Phys.* **2015**, *113*, 184–215.

(34) Mallikarjun Sharada, S.; Zimmerman, P. M.; Bell, A. T.; Head-Gordon, M. Automated transition state searches without evaluating the Hessian. *J. Chem. Theory Comput.* **2012**, *8*, 5166-5174.

(35) Maeda, S.; Ohno, K.; Morokuma, K. An automated and systematic transition structure explorer in large flexible molecular systems based on combined global reaction route mapping and microiteration methods. *J. Chem. Theory Comput.* **2009**, *5*, 2734–2743.

(36) Baker, J. An algorithm for the location of transition states. *J. Comput. Chem.* **1986**, *7*, 385-395.

(37) Fukui, K. Formulation of the reaction coordinate. *J. Phys. Chem.* **1970**, *74*, 4161-4163.

(38) Truong, T. N.; Stefanovich, E. v. A New method for incorporating solvent effect into the classical, Ab Initio molecular orbital and density functional theory frameworks for arbitrary shape cavity. *Chem. Phys. Lett.* **1995**, *240*, 253-260.

(39) Cossi, M.; Rega, N.; Scalmani, G.; Barone, V. Energies, structures, and electronic properties of molecules in solution with the C-PCM solvation model. *J. Comput. Chem.* **2003**, *24*, 669-681.

(40) Barone, V.; Cossi, M. Conductor solvent model. *J. Phys. Chem. A* **1998**, *102*, 1995-2001.

(41) Sweeton, F. H.; Mesmer, R. E.; Baes, C. F. Acidity measurements at elevated temperatures. VII. Dissociation of water. *J. Solution Chem.* **1974**, *3*, 191-214.

(42) Li, L.; Wang, -Yen; Joullie, M. M.; 79, V.; Joullié1, M. M. Synthesis of bis-benzimidazoles. *J. Am. Chem. Soc.* **1957**, *79*, 5706–5708.

(43) Xing, B.; Savadogo, O. Hydrogen/oxygen polymer electrolyte membrane fuel cells (PEMFCs) based on alkaline-doped polybenzimidazole (PBI). *Electrochem. Commun.* **2000**, *2*, 697-702.

(44) Kraglund, M. R.; Aili, D.; Jankova, K.; Christensen, E.; Li, Q.; Jensen, J. O. Zero-gap alkaline water electrolysis using ion-solvating polymer electrolyte membranes at reduced KOH concentrations. *J. Electrochem. Soc.* **2016**, *163*, F3125–F3131.

(45) Xiao, L. X.; Zhang, H. F.; Scanlon, E.; Ramanathan, L. S.; Choe, E. W.; Rogers, D.; Apple, T.; Benicewicz, B. C. High-temperature polybenzimidazole fuel cell membranes via a sol-gel process. *Chem. of Mater.* **2005**, *17*, 5328-5333.

(46) Yu, S.; Benicewicz, B. C. Synthesis and properties of functionalized polybenzimidazoles for high-temperature PEMFCs. *Macromolecules* **2009**, *42*, 8640-8648.

(47) Qian, G.; Benicewicz, B. C. Synthesis and characterization of high molecular weight hexafluoroisopropylidene-containing polybenzimidazole for high-temperature polymer electrolyte membrane fuel cells. *J. Polym. Sci. A Polym. Chem.* **2009**, *47*, 4064-4073.

(48) Walba, H.; Isensee, R. W. Acidity constants of some arylimidazoles and their cations. *J. Org. Chem.* **1961**, *26*, 2789-2791.

(49) Parrondo, J.; Wang, Z.; Jung, M. S. J.; Ramani, V. Reactive oxygen species accelerate degradation of anion exchange membranes based on polyphenylene oxide in alkaline environments. *Phys. Chem. Chem. Phys.* **2016**, *18*, 19705–19712.

(50) Wu, L.; Zhou, X.; Zhang, G.; Zhang, N.; Huang, Y.; Dai, S.; Shen, Y. Tunable OH^- transport and alkaline stability by imidazolium-based groups of poly(2,6-dimethyl-1,4-phenylene oxide) anion exchange membranes: A molecular dynamics simulation. *Ind. Eng. Chem. Res.* **2021**, *60*, 2481-2491.

(51) Pusara, S.; Srebnik, S.; Dekel, D. R. Molecular simulation of quaternary ammonium solutions at low hydration levels. *J. Phys. Chem. C* **2018**, *122*, 11204-11213.

(52) Dekel, D. R.; Willdorf, S.; Ash, U.; Amar, M.; Pusara, S.; Dhara, S.; Srebnik, S.; Diesendruck, C. E. The critical relation between chemical stability of cations and water in anion exchange membrane fuel cells environment. *J. Power Sources* **2018**, *375*, 351-360.

(53) Zadok, I.; Long, H.; Pivovar, B.; Roznowska, A.; Michalak, A.; Dekel, D. R.; Srebnik, S. Unexpected hydroxide ion structure and properties at low hydration. *J. Mol. Liq.* **2020**, *313*, 113485.

(54) Glendening, E. D.; Landis, C. R.; Weinhold, F. NBO 6.0: Natural bond orbital analysis program. *J. Comput. Chem.* **2013**, *34*, 1429-1437.

(55) Lin, B.; Dong, H.; Li, Y.; Si, Z.; Gu, F.; Yan, F. Alkaline stable C2-substituted imidazolium-based anion-exchange membranes. *Chem. Mater.* **2013**, *25*, 1858-1867.

(56) Dong, H.; Gu, F.; Li, M.; Lin, B.; Si, Z.; Hou, T.; Yan, F.; Lee, S. T.; Li, Y. Improving the alkaline stability of imidazolium cations by substitution. *ChemPhysChem* **2014**, *15*, 3006-3014.

(57) Gu, F.; Dong, H.; Li, Y.; Si, Z.; Yan, F. Highly stable N3-substituted imidazolium-based alkaline anion exchange membranes: Experimental studies and theoretical calculations. *Macromolecules* **2014**, *47*, 208-216.

TOC